

1 **IMCell^{XMBD}: A statistical approach for robust cell identi-**

2 **fication and quantification from imaging mass cytometry**

3 **images**

⁴ Xu Xiao^{1,2,#}, Naifei Su^{3,#}, Yan Kong⁴, Lei Zhang⁵, Xin Ding⁶, Wenxian Yang^{3,*}, Rongshan
⁵ Yu^{1,2,3,*}

⁶ ¹ Department of Computer Science, School of Informatics, Xiamen University, Xiamen, China

⁷ ² National Institute for Data Science in Health and Medicine, Xiamen University, Xiamen, China

⁸ ³ Aginome Scientific, Xiamen, China

⁹ ⁴ Peking University Cancer Hospital and Institute, Beijing, China

¹⁰ ⁵ School of Life Science, Xiamen University, Xiamen, China

¹¹ ⁶ Zhongshan Hospital, Xiamen University, Xiamen, China

¹² # These authors have contributed equally to this work.

¹³ * Corresponding author: rsyu@xmu.edu.cn

14

15 **Imaging Mass Cytometry (IMC) has become a useful tool in biomedical research due to its ca-**
16 **pability to measure over 100 markers simultaneously. Unfortunately, some protein channels**
17 **in IMC images can be very noisy, which may significantly affect the phenotyping results with-**
18 **out proper data processing. We developed IMCell^{XMBD1}, a highly effective and generalizable**
19 **cell identification and quantification method for IMC images. IMCell performs denoising**

¹XMBD: Xiamen Big Data, a biomedical open software initiative in the National Institute for Data Science in Health and Medicine, Xiamen University, China.

20 **by subtracting an estimated background noise value from pixel values for each individual**
21 **protein channel, identifies positive cells from negative cells by comparing the distribution**
22 **between segmented cells and decoy cells, and normalize the protein expression levels of the**
23 **identified positive cells for downstream data analysis. Experimental results demonstrate that**
24 **our method significantly improves the reliability of cell phenotyping which is essential for**
25 **using IMC in biomedical studies.**

26 **1 Introduction**

27 Analysis of the heterogeneity of cells is critical to discover the complexity and factuality of the life
28 system. Recently, single-cell sequencing technologies have been increasingly used in the research
29 of developmental physiology and disease ^{1–4}, but the spatial context of individual cells in the tissue
30 is lost due to tissue dissociation in these technologies. On the other hand, traditional immunohisto-
31 chemistry (IHC) and immunofluorescence (IF) preserve spatial context but the number of markers
32 is limited. The development of multiplex IHC/IF (mIHC/mIF) technologies, such as cyclic IHC/IF
33 and metal-based multiplex imaging technologies ^{5–8}, has enabled the detection of multiple mark-
34 ers simultaneously while preserving their spatial information. Imaging mass cytometry (IMC) ^{6,9},
35 one of the metal-based mIHC technologies, uses a high-resolution laser with a mass cytometer
36 and enables simultaneous measurement of up to 100 markers. Due to its high resolution and large
37 number of concurrent marker channels available, IMC has been proven to be highly effective in
38 identifying complex cell phenotypes and cell-cell interactions coupled with spatial locations, and
39 has been utilized in many biomedical and clinical studies on tumor or immune diseases ^{6,10–21}.

40 A number of methodological challenges must be overcome when applying IMC to clinical
41 applications in order to derive reliable cell quantification and phenotyping results from IMC. Im-
42 ages generated by a mass cytometry system are subject to noise and other acquisition artifacts
43 resulting from, e.g., sample protein degradation or signal spill-over between heavy metals ²². In-
44 strument performance can vary within a single sample, not to mention the technical variance among
45 different instruments. Besides, the antibody performance and antigen retrieval condition can dif-
46 fer between samples due to their storage time and environment, which result in protein variations
47 between and within samples. Therefore, specific data processing steps are needed to ensure mea-
48 surement of cellular markers with high resolution, quality, and reproducibility. Quality control and
49 data normalization have been incorporated into the standard operation procedures in the software
50 of the mass cytometers to convert raw signals to images ²³. Most IMC image quality control and
51 preprocessing steps are performed semi-automatically and tuned for individual datasets. Some
52 generic signal processing techniques have been applied to different datasets, including background
53 removal, hot pixels removal, and denoising by low pass filtering, etc. ^{11,24}. Data normalization has
54 also been discussed to eliminate the variation between samples ^{25,26}. Despite the progress in IMC
55 data processing tools, in practice it is still possible to obtain IMC images with very poor signal-
56 to-noise ratios (SNR) that exceed the processing capabilities of existing tools. In such cases, it
57 remains as an intricate issue to identify true positive cells from strong background noise and har-
58 monize their protein expression levels across slides from different samples or different regions of
59 interest (ROIs) from the same slide for downstream analysis.

60 In this paper, we present IMCell, a method for protein expression quantification for single

61 cells from IMC images. IMCell is able to reliably identify positive cells from highly noisy channels
62 of an IMC image, and perform expression quantification for these cells. To this end, IMCell uses
63 a Monte Carlo method to create decoy cells randomly on the potential noise regions of the image,
64 and computes the distribution of the protein expression of the decoy cells to derive the background
65 noise level of the image. The positive cells are then identified with false discovery rate (FDR)
66 control by comparing the protein expression distribution of decoy cell with that of the segmented
67 true cells. To reduce the effect of background noise on the quantification results, IMCell further
68 performs noise reduction on the IMC images with the identified background noise level. Finally,
69 the protein expression values of the positive cells are normalized to mitigate the variations of pixel
70 values across different IMC images. Our evaluation results show that IMCell can retain real signals
71 with a user-defined confidence level and eliminate sample variations, improves IMC image quality,
72 and benefits the downstream analysis.

73 **2 Results**

74 **IMCell identifies true positive cells from noise** IMCell identifies positive cells on each protein
75 channel based on FDR control with the distribution of permuted decoy cells. First, IMCell ran-
76 domly generates a large number of decoy cells on potential noise regions of each protein channel
77 (Methods, Figure 1). With the generated decoy cells, IMCell identifies positive cells by comparing
78 the distributions of cell protein expressions, calculated as the mean of pixel values of the cell, of all
79 segmented cells and decoy cells, from which the detection threshold can be set based on the target
80 FDR (Methods, Figure 1). Once the positive cells are identified on each protein channel, IMCell

81 further estimates the background noise level (Methods), which is then removed from the respective
82 IMC channel to generate a clean image for each channel.

83 We compared the performance for background noise removal of IMCell with two commonly
84 used methods, the percentile method and the median filter. The percentile method defines a lower
85 threshold T_l and an upper threshold T_h . It then removes outliers by setting pixel value to zero
86 for those lower than T_l , and setting pixel values to T_h for those higher than T_h . Here we used
87 the 1st percentile (Q_1) as T_l and the 99th percentile (Q_{99}) as T_h . Results show that the percentile
88 method removes outliers but cannot deal with noise of similar intensity values as the signal, such
89 as salt-and-pepper noise. On the other hand, the median filter is only effective in removing salt-
90 and-pepper noise but does not remove other types of noise. In addition, it tends to remove true
91 expression signals wrongly at cell boundaries, or if the true expression signals have a salt-and-
92 pepper noise-like spatial patterns. In contrast, by estimating the background noise level from
93 decoy cells randomly drawn from the potential noise regions of the image, IMCell successfully
94 removed background noise while preserving the true protein expression values from positive cells,
95 resulting in a cleaner image with significantly improved the SNR (Figure 2a, 2b).

96 We further compared the co-expression patterns of CD45, CD3 and CD4 from different
97 methods and observed that IMCell can retain true CD3 signal since most CD4 T cells expressed
98 both CD3 and CD4, while the median filter over-removed CD3 signal and the percentile method
99 failed to remove noise in the CD3 channel (Figure 2c, 2d)).

100 **IMCell reduces variations in pixel intensity and cell protein expression across IMC images.**

101 Analysis of the raw images and segmented cells show that the range of pixel intensity values and
102 the level of SNR vary significantly among samples (Figure 3a). The difference is conspicuous
103 even after performing the variance stabilizing transform, e.g., the inverse sinh transform ²⁷, on the
104 IMC images to reduce the overall range of the pixel intensities (Figure 3b). The distribution plots
105 demonstrate that the variation across samples exists not only at pixel level but also at cell level,
106 if the cell protein expressions were calculated directly from the raw images. Large inter-sample
107 distribution variation could be misleading in downstream data analysis, as the cells may cluster by
108 samples but not by cell types. In IMCell, protein expression levels are normalized across the entire
109 dataset based on the identified positive cells (Methods). Figure 3c shows the variation of intensity
110 across three samples at both pixel and cell levels after intensity normalization by IMCell.

111 **IMCell enables clustering with biological significance** To investigate the effects of different

112 IMC image preprocessing methods on downstream analysis, we applied unsupervised clustering
113 on cells generated from raw IMC images, images processed with the median filter, the percentile
114 method, and IMCell, respectively, using a same subset of proteins as features. After clustering,
115 the cell type of each cluster can be identified based on its marker expression pattern compared to
116 that of known immune and tumor cell types (Figure 4). The cell types of the cell clusters obtained
117 from raw IMC images or images processed using the percentile method can hardly be identified.
118 As the heatmap shows, some clusters have more than one relatively high cell-type-specific protein
119 expressions (Figure 4a). For example, Cluster 1 from the raw IMC images contains similar protein
120 expression level for both lymphoid (CD4) and myeloid cells (CD14, CD68), causing confusion in

121 cell type identification. The percentile method also leads to a confusing heatmap where the cell
122 types cannot be ascertained (Figure 4b). Alternatively, by applying the median filter or IMCell on
123 the raw images, the cell clustering results are more biologically significant (Figure 4c, 4d). For
124 the clustering results obtained from cells of IMC images preprocessed by the median filter, we can
125 annotate Cluster 12 as B cell, but still have difficulty to determine other two clusters (Cluster 1
126 and 10) because they contain T cell markers (e.g., CD4, CD8) and a certain amount of myeloid
127 cell markers such as CD68 and CD14. On the other hand, we are able to obtain highly specific
128 cell clusters from clustering results obtained from cells quantified with IMCell, e.g., CD4 T cell
129 (Cluster 4), CD8 T cell (Cluster 1), B cell (Cluster 3) and myeloid cell (Cluster 12, 13, 15).

130 **3 Discussion**

131 In this work, we developed IMCell which enables efficient and accurate cell quantification from
132 IMC images. Our work is based on statistical testing on the distributions of both segmented cells,
133 which are regarded as true cells identified by image segmentation software, and decoy cells. As
134 decoy cells are drawn from potential noise-only regions of IMC image with random shapes and
135 locations, it can be anticipated that its distributions will highly resemble those of negative cells (i.e.,
136 cells that don't express target proteins). Therefore, the positive cells can be reliably identified with
137 proper FDR control base on the distributions of both cells. Note that the successful application of
138 IMCell depends on the availability of information on true cell segmentation. In this work we used
139 Dice-XMBD²⁸, a deep neural network based IMC cell segmentation tool that is able to perform
140 automatic cell segmentation from IMC images without manual annotation. It is also possible to

141 use other cell segmentation tools, e.g., Ilastik ²⁹ and CellProfiler ³⁰, to perform such a task.

142 Normalization across different images is critical to align the protein expressions to the same
143 sea-level such that they can be compared in downstream data analysis. However, such normaliza-
144 tion can only be performed if the positive cells (i.e., cells expressing certain target proteins) can be
145 reliably identified. Otherwise, the normalization can falsely amplify negative cells located at noise
146 regions of the image, resulting in severe false positive issues that plague the downstream biological
147 analysis. For this reason, expression normalization is seldom performed in existing IMC process-
148 ing pipelines although significant inter-slide variations of marker protein expressions are common
149 in IMC studies. In IMCell, by rigorous FDR control, expression normalization is only performed
150 on high-confidence positive cells, thus minimizing the risk of amplification of false-positive cells.
151 As validated by visual inspection and clustering analysis, cell quantification by IMCell leads to
152 much more consistent connections between cell phenotypes and marker protein expressions. We
153 anticipate that IMCell could help to promote better usage of the IMC technologies both in research
154 labs and in clinical settings.

155 4 Methods

156 **Patients and IMC data acquisition** Melanoma cancer formalin-fixed paraffin-embedded (FFPE)
157 tissues were stained with a customized panel (35 antibodies) to generate the IMC images used in
158 this study. We excluded images containing large areas with nonspecific background staining that
159 could be caused by nonspecific antibody binding ³¹ by manual inspection using the MCD viewer

160 (V1.0.560.6). The remaining 158 images were further analyzed in the following procedures.

161 **Overview of the IMCell workflow.** IMCell consists of two main modules, denoising and normal-
162 ization (Figure 5). Firstly, raw IMC images are preprocessed and segmented by any cell segmen-
163 tation method. Then we randomly generate a number of decoy cells on the potential noise region
164 of each protein channel image. The protein expressions of the decoy cells are used to estimate
165 the background noise of the protein image. After that the protein expression distributions of all
166 segmented cells and decoy cells are compared to identify positive cells with FDR control. Next,
167 in the normalization module, to fairly compare positive cells across images, we scale the mean ex-
168 pression of positive cells from each image to the same level. More details are described as follows
169 step by step.

170 **Cell segmentation using Dice-XMBD** Single cells were identified by Dice-XMBD ²⁸ using a
171 pretrained deep neural network model, and referred to as segmented cells in this paper. Note that
172 other cell segmentation methods can also be used in the IMCell workflow. For quality control,
173 the segmented cells that cover less than 5 pixels are discarded. The cell protein expressions are
174 extracted as the mean of the pixel intensity values in each cell mask region.

175 **Preprocessing and hot pixel removal** We first applied the hyperbolic inverse sine function (arc-
176 sinh) on all the pixel intensities for each channel. The raw marker intensities output from cytome-
177 ters tend to have strongly skewed distributions with varying ranges of expression values. It is thus
178 a common practice to transform the raw marker intensities using arcsinh to make the distributions
179 more symmetric and to map them to a comparable range of expressions ^{27,32}.

180 Hot pixels were removed by filtering with a 5×5 pixel² window. If the center pixel of the
181 window was in the top 2% of all pixel intensity values in the channel and was at least $4 \times$ above
182 the median value of all pixels in the window, it will be identified as a hot pixel and its value will
183 be replaced by the median value in the window. This step reduces the scattered hot pixels' noise
184 on quantification of protein expression values for the cells.

185 **Generating decoy cells** We established the distribution of noise for each channel by generating
186 a large number (N) of decoy cells using a Monte Carlo method. To this end, we first identified
187 regions on the image that potentially contain noise-only signals without real protein expression
188 by excluding pixels with values above $0.05 \times Q_{99}$, where Q_{99} is the 99th percentile (Q_{99}) of the
189 pixel intensity values. After that, we set the value of remaining pixels to zero and smooth the noise
190 regions by applying a 5×5 median filter on the image.

191 We then fit each segmented cell as an ellipse. For each image, the mean and variance of the
192 major axis, the minor axis, and the orientation angle of all the segmented cells were calculated, and
193 these three parameters were fit using individual Gaussian models. Random parameters are drawn
194 from the distributions of the major axis, the minor axis, and the orientation, respectively, to form
195 an ellipse as a decoy cell. The decoy cell was randomly placed in the noise region of the channel
196 image, such that the center of the decoy cell was at least 5 pixels away from image boundaries.
197 The decoy cell should only lie in noise regions, i.e., all of its pixels lie in noise regions as in the
198 noise region mask. When the decoy cell lies on the border of the image, it must cover more than 5
199 pixels in the image, otherwise it will be discarded. We further filter out the decoy cell if the area

200 it covered exceeded the size range of all segmented cells. Then, the protein expression value for
201 each decoy cell was calculated as the mean of its pixel intensities in the preprocessed IMC image.

202 **Background noise removal** To eliminate the effect of different background noise profiles and
203 levels between different proteins in an IMC dataset, we removed background noise using the decoy
204 cells generated from the noise regions. For each protein channel, the mean of protein expressions
205 of all generated decoy cells was calculated, which was further subtracted from each pixel intensity
206 to remove channel-specific background noise.

Positive cells identification by FDR control Note that the segmented cells may include both positive cells and negative cells. We used a permutation test to compare the protein expression distributions between segmented cells and randomly drawn decoy cells from the noise regions, and use FDR control to identify positive cells. The FDR value can be adjusted to obtain positive cells with acceptable error-tolerant rate. The FDR of true cell identification is calculated by

$$FDR = \frac{FP}{FP + TP}, \quad (1)$$

207 where TP and FP refer to true positive and false positive, respectively. More specifically, TP refers
208 to the number of segmented cells with protein expression values larger than the threshold, while
209 FP refers to the number of decoy cells with protein expression values larger than the threshold.
210 The default value of FDR was set to 0.01, and the threshold for positive cell identification can be
211 then determined to satisfy the FDR level.

212 **Normalization of cell protein expressions** The data processing steps above are all performed on
213 individual protein channel images. As the antibody performance and the SNR can differ consid-
214 erably between FFPE tissues due to variations in tissue processing, we further normalized the cell
215 protein expression values across different samples within one IMC dataset for each protein sep-
216 arately. Denote the channel image of protein p for sample i as $I_i^{(p)}$ and the mean of the protein
217 expression values for all identified positive cells as $\mu_i^{(p)}$. Let $m^{(p)}$ denote the maximum protein
218 expression value among all identified positive cells for protein p in all samples. The cell protein
219 expression values for sample i were then scaled by factor $\frac{m^{(p)}}{\mu_i^{(p)}}$.

220 **Single cell clustering and phenotyping** High-dimensional single cell protein expression data
221 were clipped at the 99th percentile followed by min-max normalization. We selected 20 mark-
222 ers to perform cell clustering: CD45, CD3, CD4, CD8a, FoxP3, CD20, CD68, CD14, CD16,
223 CD11c, CD11b, IDO, Vimentin, α -SMA, E-cadherin, EpCAM, CA9, VEGF, PDGFRb and Colla-
224 gen. The clustering analysis consists of two consecutive steps, first, a self-organizing map (50 \times 50
225 nodes) implemented in FlowSOM (R package, v1.18.0) was used to generate several groups, then
226 a community detection algorithm by Phenograph (R package, v0.99.1) was used on the mean ex-
227 pression values of each group from FlowSOM clustering results. Cell phenotyping was determined
228 by calculating the mean of protein expressions for each cluster and compare the protein expression
229 patterns of each cluster with that of known cell types.

230 **Conflict of Interest Statement**

231 RY and WY are shareholders of Aginome Scientific. The authors declare no other conflict of
232 interest.

233 **Author Contributions**

234 WY and RY supervised the study and developed the concept. NS implemented the denoising
235 method and XX conducted experiments in evaluation and biological analysis. YK and LZ worked
236 on samples from patients. XD provided confirmatory pathology analyses. All authors wrote and
237 discussed on the manuscript.

238 **References**

- 240 1. Lähnemann, D. *et al.* Eleven grand challenges in single-cell data science. *Genome Biology*
241 **21**, 1–35 (2020).
- 242 2. Stubbington, M. J., Rozenblatt-Rosen, O., Regev, A. & Teichmann, S. A. Single-cell tran-
243 scriptomics to explore the immune system in health and disease. *Science* **358**, 58–63 (2017).
- 244 3. Potter, S. S. Single-cell rna sequencing for the study of development, physiology and disease.
245 *Nature Reviews Nephrology* **14**, 479–492 (2018).
- 246 4. Papalex, E. & Satija, R. Single-cell rna sequencing to explore immune cell heterogeneity.
247 *Nature Reviews Immunology* **18**, 35 (2018).

248 5. Tan, W. C. C. *et al.* Overview of multiplex immunohistochemistry/immunofluorescence tech-
249 niques in the era of cancer immunotherapy. *Cancer Communications* **40**, 135–153 (2020).

250 6. Giesen, C. *et al.* Highly multiplexed imaging of tumor tissues with subcellular resolution by
251 mass cytometry. *Nature Methods* **11**, 417–422 (2014).

252 7. Zrazhevskiy, P. & Gao, X. Quantum dot imaging platform for single-cell molecular profiling.
253 *Nature Communications* **4**, 1–12 (2013).

254 8. Angelo, M. *et al.* Multiplexed ion beam imaging of human breast tumors. *Nature Medicine*
255 **20**, 436–442 (2014).

256 9. Chang, Q. *et al.* Imaging mass cytometry. *Cytometry Part A* **91**, 160–169 (2017).

257 10. Damond, N. *et al.* A map of human type 1 diabetes progression by imaging mass cytometry.
258 *Cell Metabolism* **29**, 755–768 (2019).

259 11. Wang, Y. J. *et al.* Multiplexed in situ imaging mass cytometry analysis of the human endocrine
260 pancreas and immune system in type 1 diabetes. *Cell Metabolism* **29**, 769–783 (2019).

261 12. Ramaglia, V. *et al.* Multiplexed imaging of immune cells in staged multiple sclerosis lesions
262 by mass cytometry. *Elife* **8**, e48051 (2019).

263 13. Böttcher, C. *et al.* Single-cell mass cytometry reveals complex myeloid cell composition in
264 active lesions of progressive multiple sclerosis. *Acta Neuropathologica Communications* **8**,
265 1–18 (2020).

266 14. de Vries, N. L., Mahfouz, A., Koning, F. & de Miranda, N. F. Unraveling the complexity
267 of the cancer microenvironment with multidimensional genomic and cytometric technologies.
268 *Frontiers in Oncology* **10**, 1254 (2020).

269 15. Brähler, S. *et al.* Opposing roles of dendritic cell subsets in experimental gn. *Journal of the*
270 *American Society of Nephrology* **29**, 138–154 (2018).

271 16. Aoki, T. *et al.* Single-cell transcriptome analysis reveals disease-defining t-cell subsets in
272 the tumor microenvironment of classic hodgkin lymphoma. *Cancer Discovery* **10**, 406–421
273 (2020).

274 17. Jackson, H. W. *et al.* The single-cell pathology landscape of breast cancer. *Nature* **578**, 615–
275 620 (2020).

276 18. Ali, H. R. *et al.* Imaging mass cytometry and multiplatform genomics define the
277 phenogenomic landscape of breast cancer. *Nature Cancer* **1**, 163–175 (2020).

278 19. Dey, P. *et al.* Oncogenic kras-driven metabolic reprogramming in pancreatic cancer cells
279 utilizes cytokines from the tumor microenvironment. *Cancer Discovery* **10**, 608–625 (2020).

280 20. Zhang, Y., Gao, Y., Qiao, L., Wang, W. & Chen, D. Inflammatory response cells during acute
281 respiratory distress syndrome in patients with coronavirus disease 2019 (covid-19). *Annals of*
282 *Internal Medicine* (2020).

283 21. Schwabenland, M. *et al.* Deep spatial profiling of human covid-19 brains reveals neuroin-
284 flammation with distinct microanatomical microglia-t-cell interactions. *Immunity* **54**, 1594–
285 1610.e11 (2021).

286 22. Chevrier, S. *et al.* Compensation of signal spillover in suspension and imaging mass cytometry.

287 *Cell Systems* **6**, 612–620 (2018).

288 23. Lee, B. H. & Rahman, A. H. Acquisition, processing, and quality control of mass cytometry

289 data. In *Mass Cytometry*, 13–31 (Springer, 2019).

290 24. Baharlou, H., Canete, N. P., Cunningham, A. L., Harman, A. N. & Patrick, E. Mass cytometry

291 imaging for the study of human diseases—applications and data analysis strategies. *Frontiers*

292 in *Immunology* **10**, 2657 (2019).

293 25. Ijsselsteijn, M. E., Somarakis, A., Lelieveldt, B. P., Hollt, T. & de Miranda, N. F. Semi-

294 automated background removal limits loss of data and normalises the images for downstream

295 analysis of imaging mass cytometry data. *bioRxiv* (2020).

296 26. Keren, L. *et al.* A structured tumor-immune microenvironment in triple negative breast cancer

297 revealed by multiplexed ion beam imaging. *Cell* **174**, 1373–1387 (2018).

298 27. Bendall, S. C. *et al.* Single-cell mass cytometry of differential immune and drug responses

299 across a human hematopoietic continuum. *Science* **332**, 687–696 (2011).

300 28. Xiao, X. *et al.* Dice-XMBD: Deep learning-based cell segmentation for imaging mass cytom-

301 etry. *Frontiers in Genetics* **12**, 1532 (2021).

302 29. Sommer, C., Straehle, C., Köthe, U. & Hamprecht, F. A. Ilastik: Interactive learning and

303 segmentation toolkit. In *2011 IEEE International Symposium on Biomedical Imaging: From*

304 *Nano to Macro*, 230–233 (2011).

305 30. Jones, T. R. *et al.* CellProfiler Analyst: data exploration and analysis software for complex
306 image-based screens. *BMC Bioinformatics* **9**, 482 (2008).

307 31. Buchwalow, I., Samoilova, V., Boecker, W. & Tiemann, M. Non-specific binding of antibodies
308 in immunohistochemistry: fallacies and facts. *Scientific Reports* **1**, 1–6 (2011).

309 32. Bruggner, R. V., Bodenmiller, B., Dill, D. L., Tibshirani, R. J. & Nolan, G. P. Automated
310 identification of stratifying signatures in cellular subpopulations. *Proceedings of the National
311 Academy of Sciences* **111**, E2770–E2777 (2014).

312 **Figure captions**

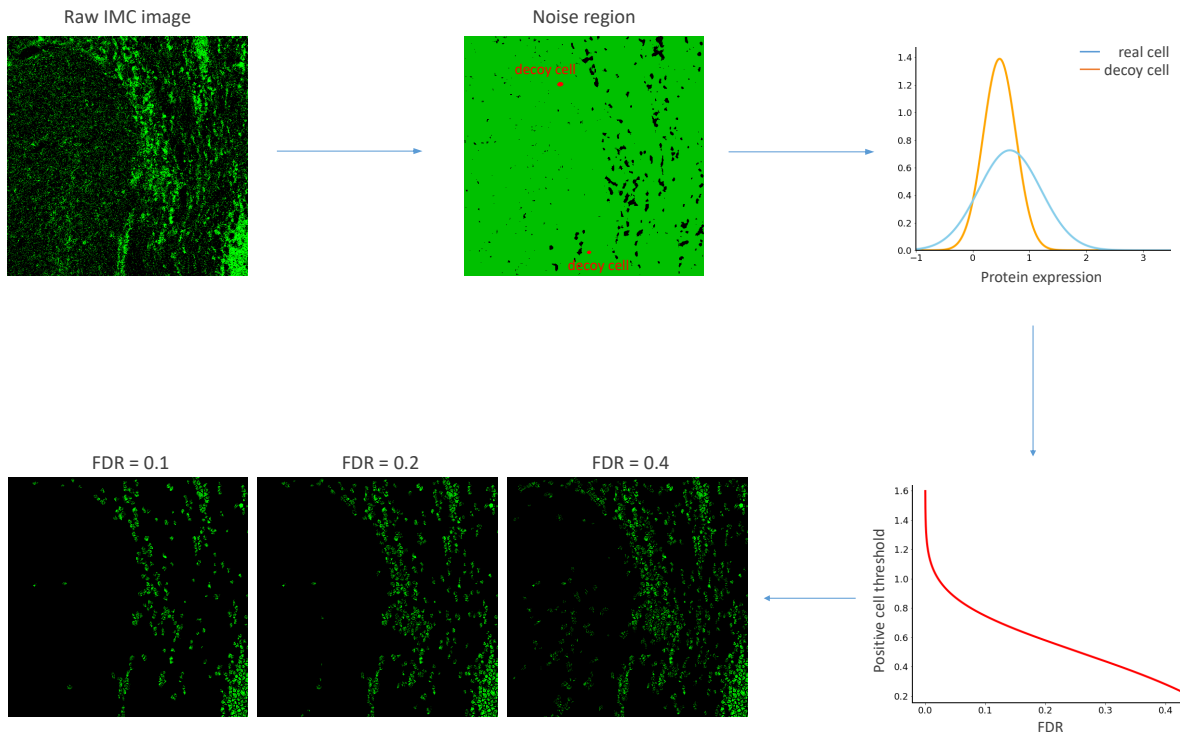


Figure 1: Positive cells identified by IMCell with different FDR control (sample: 76 ROI18, protein: CD74).

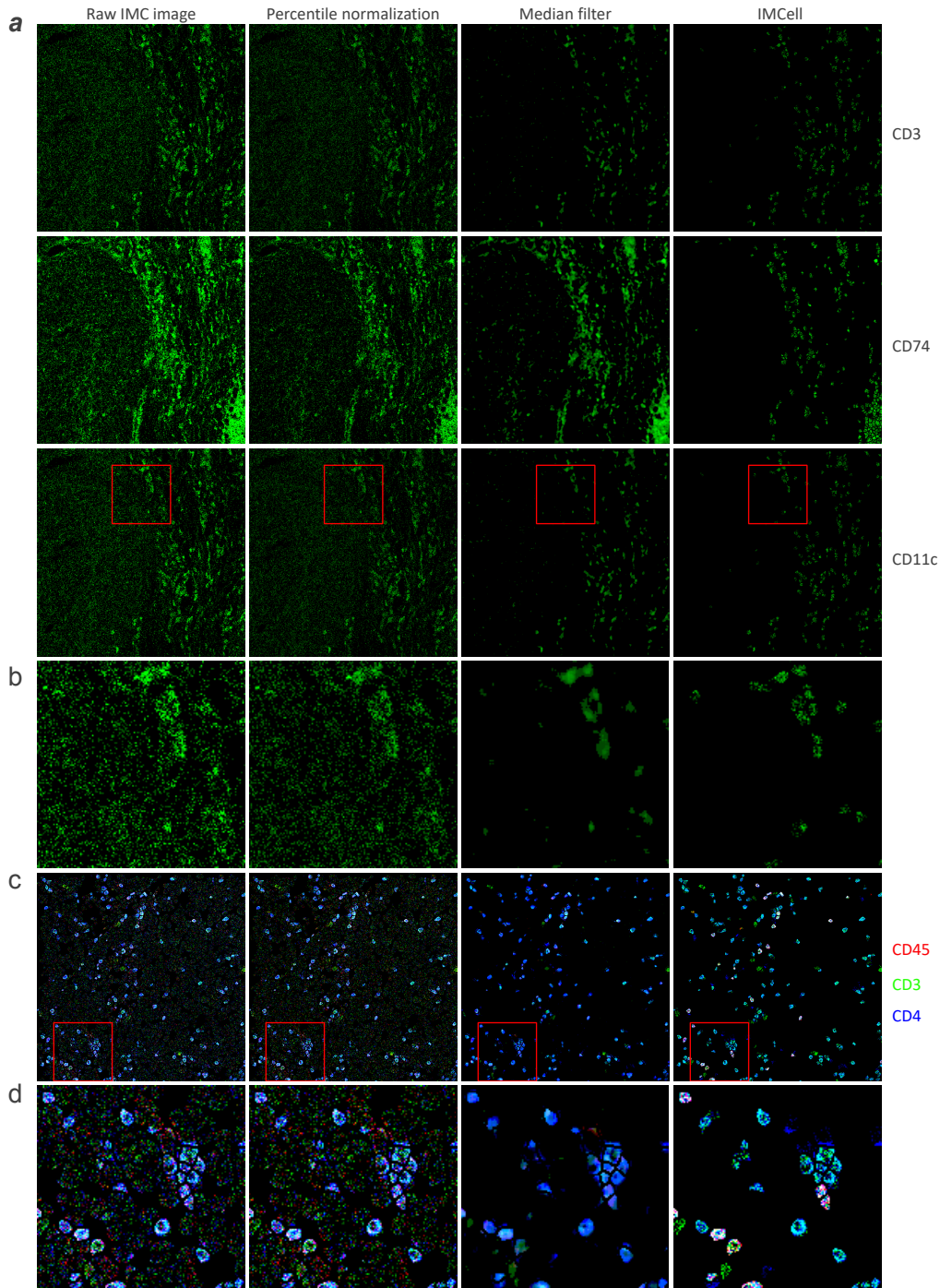


Figure 2: Performance evaluation of different methods. (a) Comparisons of cell identification results from raw IMC images, with 1st-99th percentile method to remove outliers, with median filter to remove salt-and-pepper noise, and with IMCell (sample: 76 ROI18). The red box marks the zoomed in areas on the below side (b) depicting the CD11c marker. Expression pattern of multi-markers (CD45, CD3, and CD4) in the whole images (c) and zoom-in areas (d).

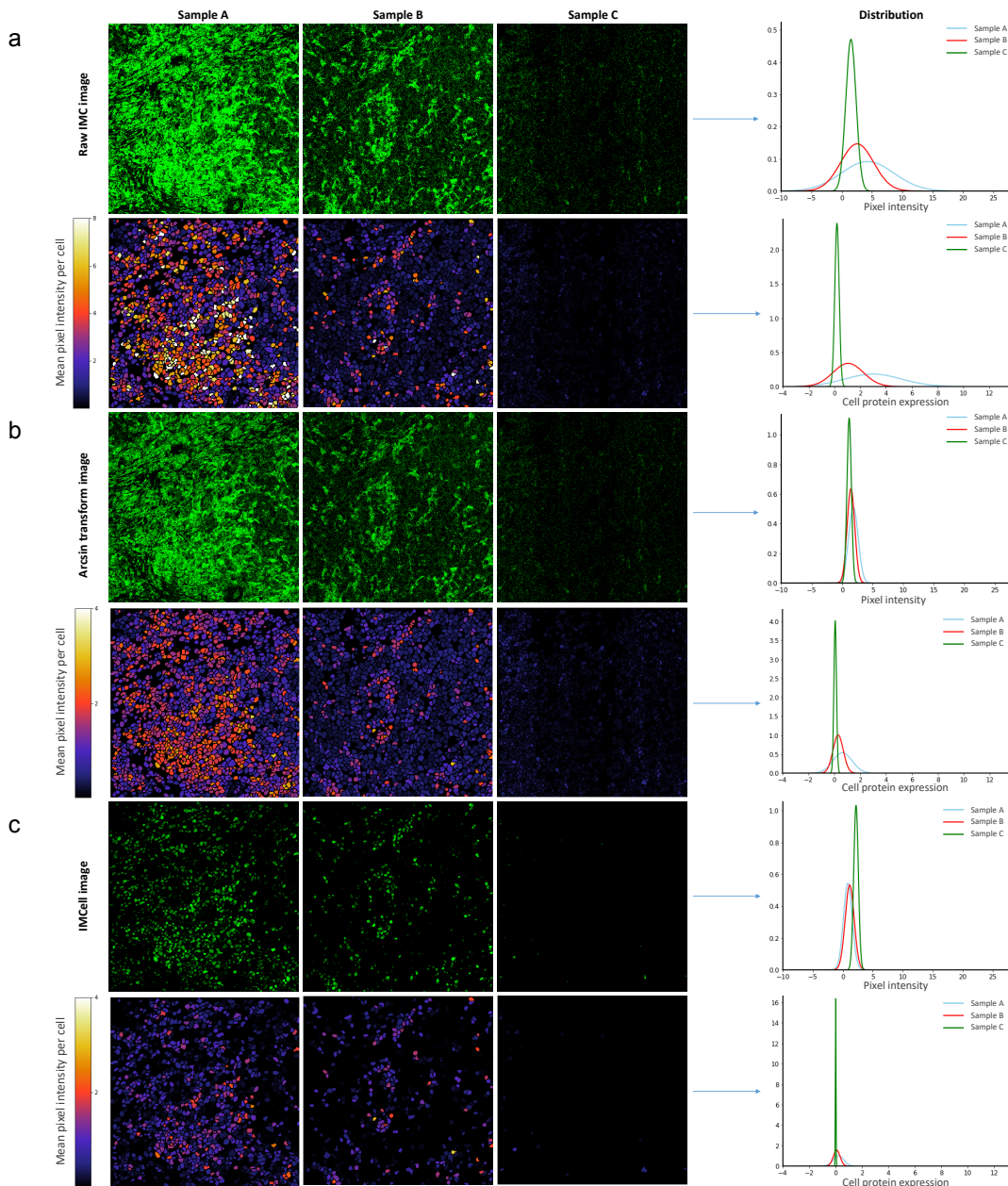


Figure 3: Variation of pixel intensity and cell protein expression across three samples (sample A: 65 ROI13, sample B: 65 ROI18, sample C: 33 ROI11). The left column shows (a) the pixel intensity (first row) and cell protein expression (second row) from the raw images, (b) the pixel intensity (first row) and cell protein expression (second row) from arcsinh-transformed images, and (c) the pixel intensity (first row) and cell protein expression (second row) from images processed by IMCell. The right column plots the distribution of the corresponding value (i.e., pixel intensity and cell protein expression).

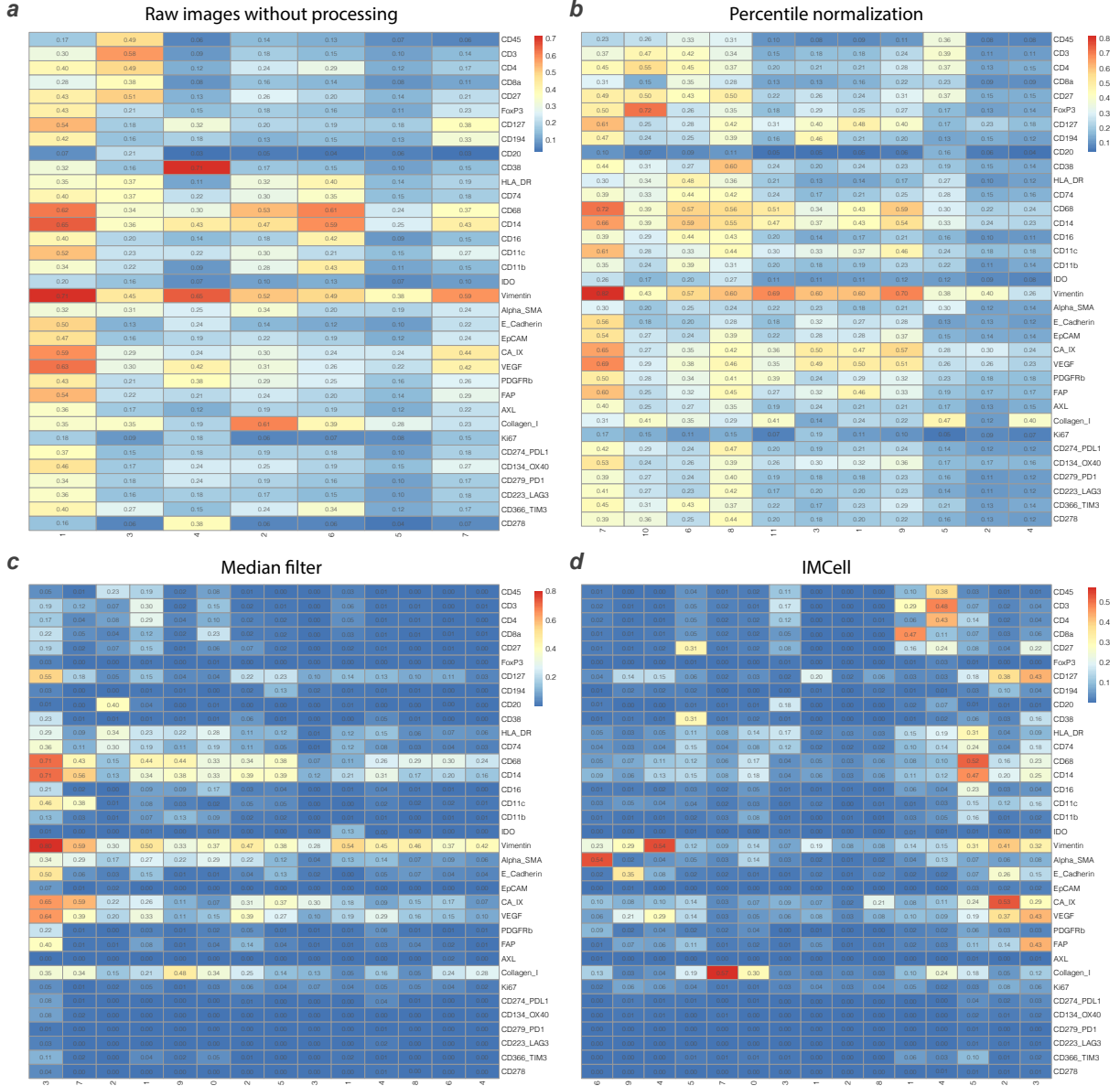
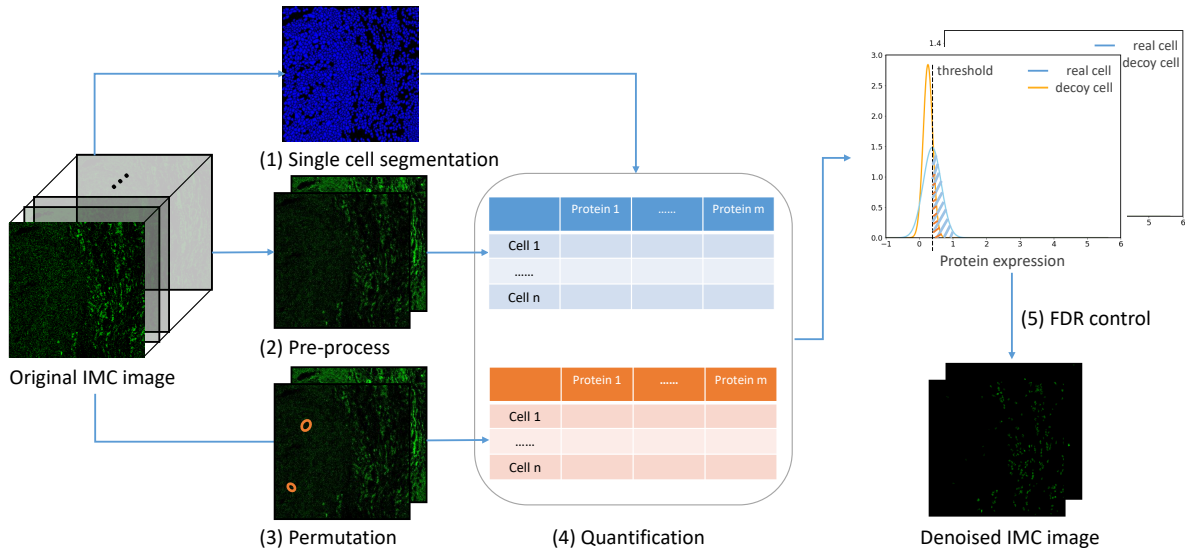


Figure 4: Clustering result from different methods. Heatmap showing mean value of normalized protein expression in each cluster. The high-dimensional single cell expression data were generated from (a) raw IMC images, (b) with 1^{st} - 99^{th} percentile method to remove outliers, (c) with median filter to remove salt-and-pepper noise, and (d) with IMCell.

(a) Denoise



(b) Normalization

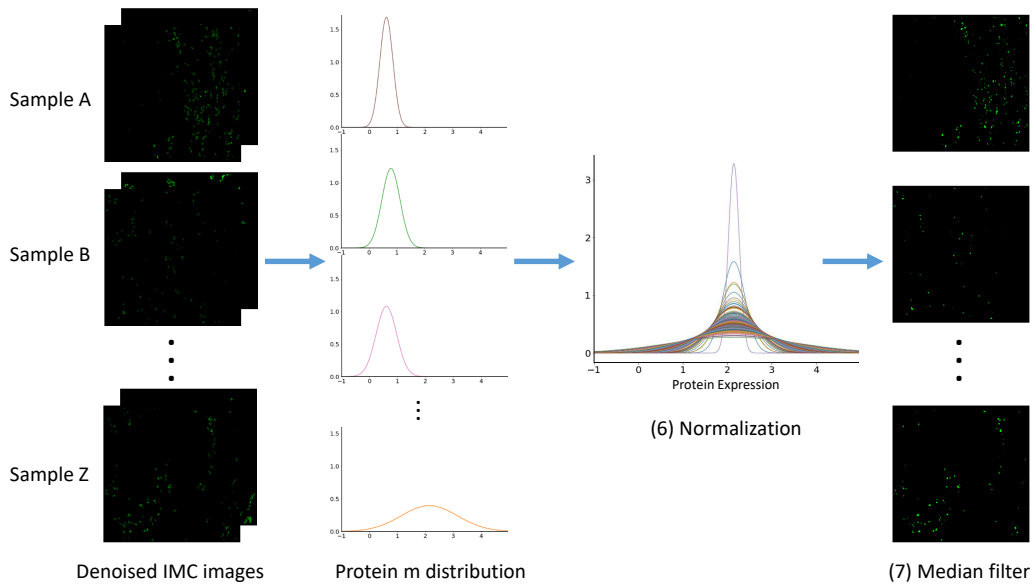


Figure 5: The workflow of IMCell consists of (a) denoising and (b) normalization. The workflow includes the following procedures, (1) single cell segmentation by Dice-XMBD, (2) image pre-processing and hot pixel removal, (3) random generation of decoy cells in potential noise regions, (4) protein quantification for segmented cells and decoy cells, (5) identifying positive cells with FDR control, (6) normalization by scaling using the mean of protein expression of positive cells, and (7) apply the median filter on the denoised and normalized images.